Title

Understanding the links between composition, polyhedral distortion, and luminescence properties in green-emitting Î²-Si$_{6-z}$Al$_z$O$_z$N$_{8-z}$:Eu^{2+}...

Authors

Cozzan, Clayton
Laurita, Geneva
Gaultois, Michael W
et al.

Peer reviewed

Journal Name

Understanding the links between composition, polyhedral distortion, and luminescence properties in green-emitting β-Si$_{6-z}$Al$_z$O$_z$N$_{8-z}$:Eu^{2+} phosphor

Clayton Cozzan,[a,b,c] Geneva Laurita,[d] Michael W. Gaultois,[b,c] Marcus Cohen,[b] Alexander A. Mikhailovsky,[e] Mahalingam Balasubramanian,[f] and Ram Seshadri[*a,b,c,e]

Inorganic phosphor materials play a crucial role in the creation of white light from blue and near-UV solid-state light-emitting diodes. Understanding the intricacies of phosphor structure is key for setting the stage for improved, more efficient functionality. Average structure and coordination environment analysis of the robust and efficient green-emitting phosphor, β-SiAlON:Eu^{2+} (β-Si$_{6-z}$Al$_z$O$_z$N$_{8-z}$Eu$_{0.009}$), are combined here with a range of property measurements to elucidate the role of Al content (z) on luminescence properties, including the red shift of emission and the thermal quenching of luminescence as a function of increasing Al content z. Average structure techniques reveal changes in polyhedral distortion with increasing z for the 9-coordinate Eu site in β-SiAlON:Eu^{2+}. X-ray absorption near edge structure (XANES) is used to confirm that the majority of the activator Eu is in the Eu^{2+} state, exhibiting the symmetry-allowed and efficient $4f^75d^0 \longrightarrow 4f^65d^1$ transitions. Room temperature and temperature-dependent luminescence indicate an curious increase in thermal stability with increasing z over a small range due to an increasing barrier for thermal ionization, which is correlated to an increase in the quantum yield of the phosphor.

1 Introduction

Since the first development of affordable and efficient blue light-emitting diodes (LEDs) by Nakamura and coworkers,[1] solid-state white lighting is rapidly replacing other types of light sources.[2] Crucial to the success of this technology are inorganic phosphors that partially convert radiation from the solid-state source to longer wavelengths.[3] One of the strategies for creating white light is to use a near-UV or UV source to excite a mixture of red-, green-, and blue-emitting phosphors to render warm white light with high color rendering indices.[4] For this approach, a green-emitting phosphor of particular interest is β-SiAlON:Eu^{2+}. This phosphor displays excitation from the near-UV to blue with high

quantum yields[5] due to the rigid parent Si–N tetrahedral framework in this solid solution phosphor.[6] Like other solid solution phosphors, the optical properties can be chemically tuned.[7–9] High lattice rigidity[10,11] leads to high efficiencies at small Al concentrations (most closely resembling the Si$_3$N$_4$ lattice), with rigidity decreasing for more Al substitution.[5,6] For future high-power lighting applications,[12] the thermal stability and high efficiency of β-SiAlON:Eu^{2+} render it a suitable phosphor for generating light using blue laser diode excitation.[13]

It is well-known that both the host structure and the local coordination environment of the emission center in phosphors dictate the emission behavior.[3] β-SiAlON:Eu^{2+} crystallizes in the Si$_3$N$_4$-type structure (space group $P6_3$, no. 173).[6] A large size mismatch between cations in the structure and the Eu^{2+} cation suggests that the luminescence center (Eu^{2+}) substitutes on an interstitial site, which was confirmed by scanning transmission electron microscopy (STEM)[14] and supported separately by density functional theory (DFT) used in conjunction with Eu L_3 extended X-ray absorption fine structure (EXAFS)[6], which is challenging both due to the difficulty of modeling f-electrons and the inherently low amount of Eu in the system. Both investigations provided evidence that the Eu^{2+} substitutes in the channel on the 2a Wyckoff site with local distortions present.[6,14] Furthermore, the inclusion of the rare earth necessitates changes in the Si:Al and N:O ratios

[a] Materials Department, University of California, Santa Barbara, California 93106, United States. Fax: 805-893-6129; Tel: 805-893-6129; E-mail: seshadri@mrl.ucsb.edu
[b] Materials Research Laboratory, University of California, Santa Barbara, California 93106, United States.
[c] Mitsubishi Chemical Center for Advanced Materials, University of California, Santa Barbara, California 93106, United States.
[d] Department of Chemistry, Bates College, Lewiston, Maine 04240, United States.
[e] Department of Chemistry and Biochemistry, University of California, Santa Barbara, CA 93106, United States.
[f] X-ray Science Division, Advanced Photon Source, Argonne National Laboratory, Argonne, Illinois 60439, United States.

to maintain charge neutrality, which in turn influences the coordination environment of the rare earth. The consequences on the β-SiAlON structure for small Al/O substitutions were recently investigated experimentally using synchrotron X-ray diffraction and ^{27}Al MAS NMR coupled with DFT calculations of NMR parameters and defect structure energetics.[15] Separately, computational studies predicted effects of Al/O substitution on the properties of β-SiAlON:Eu^{2+} phosphors.[16]

These recent first principles calculations by Wang *et. al.* sought to establish chemical rules for the β-SiAlON:Eu^{2+} system as well as describe the origins of the high quenching resistance, the emission peak characteristics, and the changes in emission wavelength as a function of z in β-Si$_{6-z}$Al$_z$O$_z$N$_{8-z}$Eu^{2+} for fixed Eu doping.[16] Using DFT, the authors observed that with increasing z ($z = 0.125$ to $z = 0.167$), the Eu-N/O bond lengths increased and distorted the dopant site, which was assigned a 9-coordinate Eu-N/O$_9$ polyhedron in the $2a$ Wyckoff position. In their calculations, broadening of the emission peak and a red shift due to a larger crystal field splitting were observed due to these distortions in the Eu^{2+} environment. A slight decrease in band gap was also observed with increasing z, likely also contributing to the red shift. Calculations on the thermal ionization barrier for a fixed Eu amount interestingly observed that the barrier increased from $z = 0.125$ to $z = 0.167$ and then decreased at z values greater than $z = 0.167$ due to an increasing gap between the $5d$ levels and the conduction band of the host lattice. This is the first report of such behavior and offers an interesting compositional range to experimentally target for the highest performing β-SiAlON:Eu^{2+} phosphors.

In the current work, we present the first experimental verification of red shift, emission broadening, and thermal stability increases for small z ranges in phase pure and highly efficient β-Si$_{6-z}$Al$_z$O$_z$N$_{8-z}$Eu^{2+} phosphors. Samples with fixed nominal Eu content (Eu$_{0.009}$) and systematically varying Al/O content ($z = 0.050$, $z = 0.075$, and $z = 0.125$) were studied. The solubility of rare earth ions in the host lattice is limited by the stability of the cation in the interstitial site,[6,17] rendering traditional techniques such as X-ray diffraction not capable of direct observation of the precise dopant atom location within the channels. Synchrotron X-ray diffraction[15] can be used to probe average structure and is applied here to investigate any links between average structure changes in the Eu coordination environment location in the crystal and the observed physical properties. X-ray absorption near edge structure (XANES) of the Eu L_3 edge shows the oxidation state of the Eu in the different samples is constant (Eu^{2+}:Eu^{3+} remains the same) across the z range studied presently. It was hypothesized that an optimal Al^{3+}/O^{2-} concentration used to charge balance Eu^{2+} could be targeted to achieve high quantum yield and good thermal stability. Room temperature and temperature dependent photoluminescence measurements were conducted to analyze the photoluminescence quantum yield (PLQY) and thermal stability of the phosphors as a function of z, with the highest luminescence and thermal stability observed for $z = 0.125$. Our work supports the findings of Wang *et. al*[16], indicating a red shift and broadening of the emission spectra. We find the trend of polyhedral distortion as a function of z varies depending on the assigned location of Eu along the

c-axis of the $2a$ site, and bond valence sum calculations suggest this is not in the direct center of the channel, *i.e.*, a 12-coordinate polyhedral site (distortion is observed for a Eu-N/O$_9$ polyhedra and not for a Eu-N/O$_{12}$ polyhedron). The current work observes that if the dopant atom resides in the energetically and valency favored Eu-N/O$_9$ polyhedron, trends in distortion of the luminescent center explain the experimentally observed red shift, emission broadening, and increasing thermal stability as a function of Al content, with quantum yield shown to follow the same trend.

2 Methods

Powders of α-Si$_3$N$_4$, Al$_2$O$_3$, and Eu$_2$O$_3$ were ground with nominal stoichiometry Si$_{6-z}$Al$_z$N$_{8-z}$O$_z$Eu$_{0.009}$ ($z = 0.050$, $z = 0.075$, and $z = 0.125$) in an alumina pestle, with charge balancing of the Eu^{2+} achieved via co-substitution of Al^{3+} and O^{2-}. The powders were heated in a boron nitride crucible at 2223 K for 12 h under N$_2$ (>99.9995%) at a pressure of 0.92 MPa and annealed in argon for 8 h before being ground into a fine powder and washed using a mixture of HNO$_3$ and HF.

Collection and analysis of synchrotron X-ray diffraction data as related to this work are described elsewhere.[15] The polyhedral distortion index (D) and bond valence sum (BVS) were calculated based on bond lengths as defined by Baur[18] and implemented using the open-source crystallographic software VESTA.[19] Eu L_3 edge spectra were collected using beamline 20-BM at the Advanced Photon Source, Argonne National Laboratory. Samples were irradiated using an unfocused X-ray beam, and fluorescence spectra at 295 K were collected from powder encapsulated in Kapton$^\circledR$ tape oriented at 45° using a 13-element Ge detector perpendicular to the incident X-ray beam. The incident photon energy was calibrated using the Fe K absorption energy of Fe metal foil (E$_0$ = 7112 eV), and monitored throughout the experiments using the Eu L_3 absorption energy of Eu$_2$O$_3$ powder (E$_0$ = 6971 eV) collected concurrently in transmission mode. The instrumental resolution is 1 eV at these energies. Data were processed using the Demeter software suite.[20]

Room temperature photoluminescence spectra and photoluminescence quantum yield (PLQY) were measured using a fluorescence spectrometer (Horiba, Fluoromax 4). Phosphors were thoroughly mixed by 25-wt % in a silicone matrix (Momentive, RTV-615) using a high speed mixing system (FlackTek Inc., DAC 150.1 FVZ-K) at 1500 rpm for 2 min, and subsequently deposited on a 100 mm^2 fused silica substrate (Chemglass) and heated at 398 K for 15 min in a box furnace to accelerate the curing process. Phosphors encapsulated in a silicone matrix were then placed in a 15 cm diameter, Spectralon$^\circledR$-coated integrating sphere (Horiba, Quanta-ϕ) and excited using light with a wavelength of 405 nm and 450 nm generated by a 150 W continuous output, ozone-free xenon lamp. Slit widths for the excitation and emission monochromaters were held constant at 2.00 nm, and a metallic neutral density filter (Newport) was used. The wavelength spread, or bandpass (nm), is the resolution and is calculated by multiplying the slit width (mm) by the dispersion (4.25 nm/mm for the FluoroMax-4). The bandpass for a 2 nm slit size is calculated to be 8.5x10^{-6} nm. Therefore, reported differences of <1 nm are well resolved using the current experimental configu-
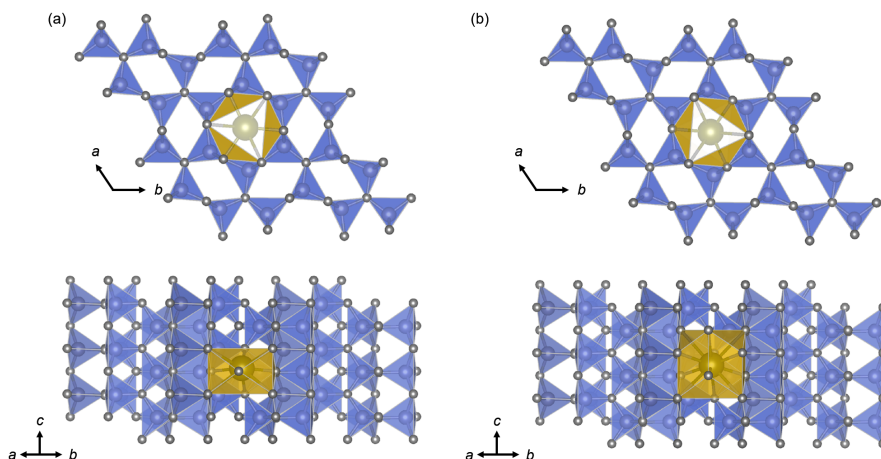
Fig. 1 Hexagonal $P6_3$ (no. 176) crystal structure of Eu^{2+} doped β-$Si_{6-z}Al_zO_zN_{8-z}$ with the Eu coordination sites highlighted in yellow. (a) Eu environment in the $2a$ Wyckoff site with an atomic position of $(0, 0, \frac{1}{3})$ results in a 9-coordinate site whereas (b) an atomic position of $(0, 0, \frac{1}{2})$ results in a 12-coordinate site. Coordination polyhedra are defined by Eu–O/N bonds under 3.45 Å.

ration. Quantum yield was calculated based on the work by de Mello *et al.*[21] The temperature dependence of the PLQY was measured from 77 K to 503 K in 30 K increments using a home-built fluorometer with a cryostat sample stage for low temperatures and a heating stage for high temperatures. Samples were prepared in the same manner described for room temperature measurements.

3 Results and discussion

Eu^{2+} doped β-$Si_{6-z}Al_zO_zN_{8-z}$ consists of densely packed, corner sharing $(Si,Al)(O,N)_4$ tetrahedra that crystallize in the hexagonal space group $P6_3$ (no. 176) with a channel along the c-axis. The likelihood that the dopant is located in this channel in the $2a$ Wyckoff site has been experimentally verified through STEM[14] and EXAFS studies[6]. However, this is not a special position, as the $2a$ site in this space group is located at $(0, 0, c)$, and the precise location of the Eu dopants along the channel has not been experimentally reported. DFT results indicated that for the (001) plane, the lowest energy region lies in the center of the channel in the a, b direction, and the energy increases as one moves away from the channel.[6] The $2a$ site is large potential well with the dopant in the $(0, 0, c)$ position. From a chemical standpoint, shifting the atom in the a or b direction results in more over-bonding due to the shorter bonds and a higher BVS, and is therefore less likely than the $(0, 0, c)$ position. Therefore, specific positions along the channel in the $(0, 0, c)$ positions are evaluated in the present work using BVS and D.

In the structure of in β-$Si_{6-z}Al_zO_zN_{8-z}$, Al substitutes on the Si site and O substitutes on the N site. For z contents evaluated presently, oxygen bonds are likely to influence the local dopant environment, which is denoted as Eu-N/O$_9$ in the present work. The in-channel c position is of importance when defining the polyhedral environment of the Eu, as is illustrated in Figure 1. For defined Eu-N/O bond lengths of <3.45 Å, an atomic position of $(0, 0, \frac{1}{3})$ results in a 9-coordinate site (Figure 1a) whereas an atomic position of $(0, 0, \frac{1}{2})$ results in a 12-coordinate site (Fig-
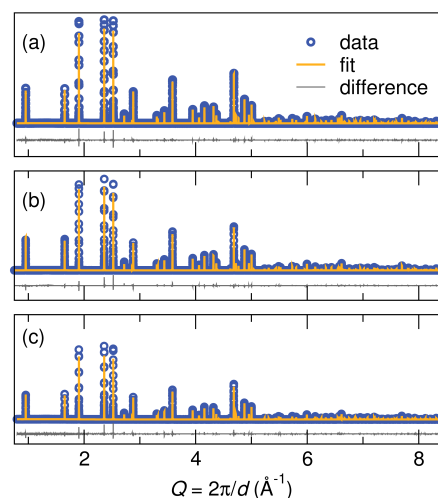

Fig. 2 Rietveld fits of synchrotron X-ray data reported in Cozzan *et al.*[15] for the series β-$Si_{6-z}Al_zO_zN_{8-z}$ [(a) $z = 0.050$, (b) $z = 0.075$, and (c) $z = 0.125$]. All samples are phase pure and indexed to the $P6_3$ space group.

ure 1b). Therefore the location within the channel must be considered when discussing the coordination environment of the activator ion.

Our recent analysis on synchrotron X-ray data of β-$Si_{6-z}Al_zO_zN_{8-z}$ ($z = 0.050$, $z = 0.075$, and $z = 0.125$), Rietveld fits shown in Figure 2, revealed an overall increase in the unit cell volume with increasing z.[15] This was in agreement with the first principles calculations by Wang *et. al.*, where the volume and average bond length increased with increasing z due to longer Al–N and Al–O bonds when compared to Si–N bonds.[16] In addition to an increase in the unit cell volume, the first principles study addressed the effect of the c position of the Eu in the $2a$ channel, finding changes in the relative energy of the β-$Si_{6-z}Al_zO_zN_{8-z}$ structure as a function of the fractional c coordinate of Eu. Based on this work they determined the lowest-energy structure con-
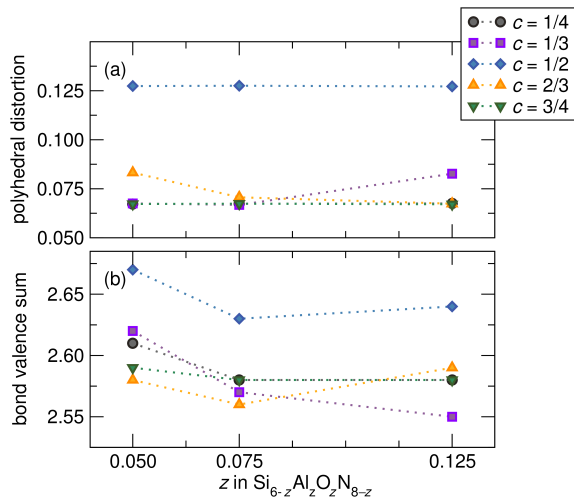
Fig. 3 (a) Polyhedral distortion of the Eu coordination polyhedra as a function of Al/O content for defined positions of $(0, 0, c)$ in the $2a$ Wyckoff position. Positions of $c=\frac{1}{4}$, $c=\frac{1}{2}$, and $c=\frac{3}{4}$ result in a minimal change in distortion with increasing Al/O content, while $c=\frac{1}{3}$ and $c=\frac{2}{3}$ result in increasing and decreasing distortion with Al/O content, respectively, highlighting the importance of the in-channel location of the Eu^{2+} activator ion. Bond valence sum (BVS) calculations indicate that for all compositions, a c location off of the center of the channel ($c=\frac{1}{2}$) results in Eu^{2+} being closer to the 2+ valency, suggesting Eu does not sit in the center of the site along the c-axis.

Table 1 Select structural data obtained from Rietveld refinements of X-ray synchrotron diffraction data for β-$Si_{6-z}Al_zO_zN_{8-z}$ with $z = 0.075$ as reported in our previous study.[15] Numbers in parentheses show standard deviation on the last number. Si/Al and O2/N2 c parameters reported to illustrate approximate location of $(000l)$ plane used to estimate the c positional parameter of Eu^{2+} based on guidelines set by Wang *et al.*[16]

Al content (z)	0.050	0.075	0.125
Cell a (Å)	7.60584(1)	7.60692(2)	7.60853(2)
Cell c (Å)	2.90844(3)	2.90903(3)	2.91011(3)
Cell V (Å³)	145.709(2)	145.780(2)	145.896(2)
Si/Al positional c	0.291(5)	0.250(3)	0.290(5)
O2/N2 positional c	0.281(7)	0.238(6)	0.28(5)

sists of an Eu dopant that is in the same $(000l)$ plane as the Al and O atoms and determined a polyhedral distortion of the resulting 9-coordinate Eu site with an increase in Al and O substitution. Through this work they outlined three rules for achieving a low-energy β-$Si_{6-z}Al_zO_zN_{8-z}$ structure: (1) All O must occupy the $2c$ Wyckoff sites, (2) all O must have at least one Al neighbor, and (3) all Al, O, and Eu must be in the same $(000l)$ plane.

In the present work, the average atomic positions calculated from Rietveld refinements have been used to calculate bond distances, polyhedral volumes, and D as a function of Al/O content for chosen positions of $(0, 0, c)$ in the $2a$ Wyckoff position (Figure 3a) in the doped β-$Si_{6-z}Al_zO_zN_{8-z}$ unit cell. The terms Eu site and $2a$ site are referred to interchangeably in the present work. By studying characteristics of the bonding environment of the dopant site at chosen c values, such as coordination number and bond valence sum (BVS), our average structure data allows for an understanding of the most likely position in the channel despite not directly probing the dopant in the material. Eu coordi-
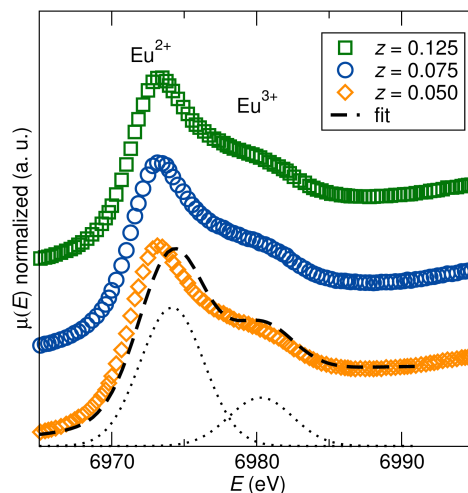

Fig. 4 XANES of the Eu L_3 edge shows the valence state of Eu is 81% ($\pm$ 5%) Eu^{2+} for the series of β-$Si_{6-z}Al_zO_zN_{8-z}$:$Eu_{0.009}$ with varying z. A representative XANES fit is shown (dashed line) for the $z=0.050$ sample with individual Gaussian components for Eu^{2+} and Eu^{3+} (dotted lines) shown and arctangent steps not shown for clarity.

nation polyhedra were defined by Eu-N/O bond lengths <3.45 Å, resulting in a 9-coordinate site for $c=\frac{1}{4}$, $c=\frac{1}{3}$, $c=\frac{2}{3}$, and $c=\frac{3}{4}$ and a 12-coordinate site for $c=\frac{1}{2}$ in all compositions. It is observed that positions of $c=\frac{1}{4}$, $c=\frac{1}{2}$, and $c=\frac{3}{4}$ result in a minimal change in distortion with increasing Al/O content, while $c=\frac{1}{3}$ and $c=\frac{2}{3}$ result in increasing and decreasing distortion with Al/O content, respectively. To provide more insight on the probable location of the Eu within the channel, BVS as a function of Al/O content were calculated for the defined positions (Figure 3b).[22] Previous work using EXAFS demonstrated that a BVS of 2 is obtained when long bond lengths (4 Å) are considered.[6] There is some ambiguity in the precise determination of the local dopant bonding environment due to such low Eu, and the exact position of the Eu along the channel has not yet been directly observed. BVS as utilized in the current work is therefore a guide to understanding the bonding environment of the $2a$ site on average in structures varying as a function of Al/O content, suggesting which location of the Eu is the least over-bonded. All positions result in over-bonded Eu with BVS above 2.5 (compared to the optimal BVS of 2.0), but this is slightly relieved when Eu does not occupy the center of the channel ($c=\frac{1}{2}$). Deviations from the ideal BVS of 2 as expected for Eu^{2+} might also arise due to local disorder of the O in the polyhedron that is not captured using crystallographic techniques. Following the Eu positional rules outlined by the previous first principles work,[16] a c position of approximately 0.3 would place Eu in the proper $(000l)$ plane for our refined structures (Table 1) with bonds along the plane. This value is closest to the calculated $c=\frac{1}{3}$, suggesting that an increase in the polyhedral distortion of the 9-coordinate Eu site occurs with increasing Al/O content. The current work provides experimental support for investigating Eu-N/O_9 polyhedra, which corroborates recent work by other authors.[16,23]

XANES of the Eu L_3 edge was collected to observe the valence state of Eu in the phosphors (Figure 4). The majority of Eu in the
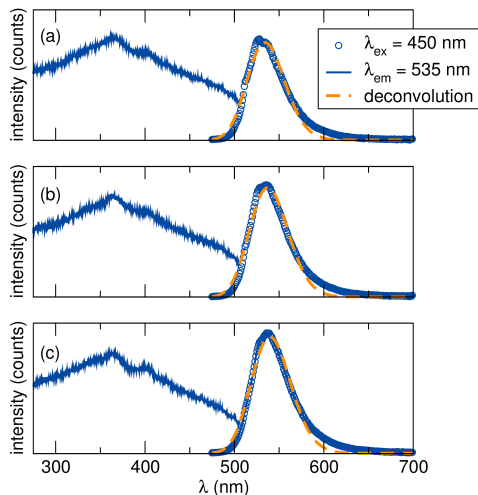
Fig. 5 Emission spectra deconvolution with one Gaussian peak shape for (a) $z = 0.050$, (b) $z = 0.075$, and (c) $z = 0.125$ show the contributions of the activator site for each phosphor, with one peak accounting for one unique position of Eu^{2+} in the unit cell. The tail of the emission profile is not captured by a single Gaussian, likely due to a distribution of dopant positions due to small fluctuations in channel position and/or small changes in the dopant environment due to local changes in N/O distribution. Intensity is plotted in counts (arbitrary units).

Table 2 Peak maximum and FWHM of the emission spectra. Increasing z shows a small red shift in the emission.

Al content z	maximum (nm)	FWHM (nm)
0.050	531	46
0.075	535	46
0.125	537	48

samples is in the optically active, *i.e.*, allowed 4f⟶5d transitions, Eu^{2+} state due to the highly reducing processing atmosphere of N_2 (>99.9995%) at a pressure of 0.92 MPa and the subsequent argon anneal. Quantitative fitting of XANES data using two arctangent steps and two Gaussian functions was performed using Eu_2O_3 as a reference, resulting in a calculated 81% of Eu^{2+}, and 19% Eu3+ ($\pm 5\%$) for each sample. A representative XANES fit with the individual Gaussian components for Eu^{2+} and Eu^{3+} is shown in Figure for the $z=0.050$ sample (arctangent steps not shown for clarity). The relative amount of $Eu^{2+}:Eu^{3+}$ is constant regardless of z, indicating that any observed differences in the optical properties with varying z is due to structural changes and not to the $Eu^{2+}:Eu^{3+}$ ratio.

Eu^{2+} doped β-$Si_{6-z}Al_zO_zN_{8-z}$ displays green emission and is readily excited by $\lambda_{ex} = 405$ nm (near UV) and $\lambda_{ex} = 450$ nm (blue) due to broad excitation,[24–26] with excitation (line) and emission (circles) profiles for $\lambda_{ex} = 450$ nm for different z values shown in Figure 5. The emission spectra were deconvoluted on an energy scale (cm^{-1}) using one Gaussian peak corresponding to one crystallographically unique luminescent center in the unit cell. The tail of the emission profile is not captured by a single Gaussian, and is likely due to a distribution of dopant positions due to small fluctuations in channel position in the phosphor. Additionally, small changes in the dopant environment due to local changes in N/O can result in a distribution of local ac-
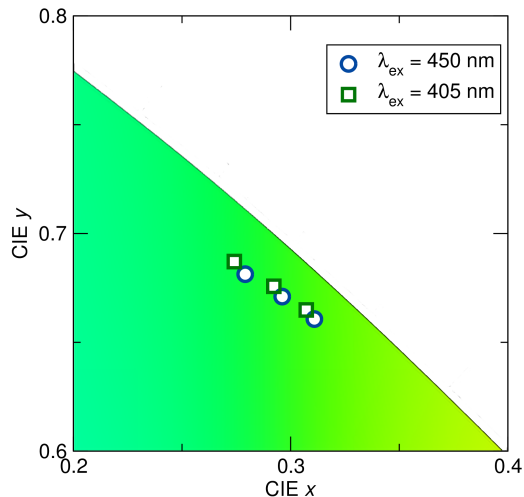

Fig. 6 CIE coordinates on a section of the 1931 CIE diagram for $\lambda_{ex} = 405$ nm (squares) and $\lambda_{ex} = 450$ nm (circles), with an arrow indicating increasing z in β-$Si_{6-z}Al_zO_zN_{8-z}:Eu_{0.009}$ at room temperature. Systematic change for the series is due to a red shift in the emission with increasing z.

tivator environments. The emission and broad excitation spectra are due to the allowed $4f^65d^1 \longrightarrow 4f^7$ transition in Eu^{2+}. Values for the maximum emission wavelength and full width at half maximum (FWHM) of the Gaussian peak shape fits are shown in Table 2. There is a clear red shift in emission for increasing amounts of Al substitution. The observed optical behavior in β-$Si_{6-z}Al_zO_zN_{8-z}$ with increasing z is not well explained by average bond lengths or polarizability of nitrogen,[3] as a red shift is observed with both increasing bond length and with increasing O. It has been experimentally observed that polyhedral distortion can alternately dominate crystal field splitting in some garnet-based phosphor systems, where a red shift in the emission was correlated to the distortion of the luminescence center.[27] A red shift in the emission due to polyhedral distortion was calculated by Wang *et. al.*[16] assuming that Eu^{2+} occupies the channel at approximately $(0,0,\frac{1}{2})$, which is probable based on our own BVS calculations. It is therefore possible that polyhedral distortion is a reasonable mechanism for the red shift in β-$Si_{6-z}Al_zO_zN_{8-z}$ with increasing z.

The red shift can also be visualized by the Commission Internationale de l'Éclairage (CIE) (x,y) coordinates for the phosphor (Figure 6), which show an increase in CIE x and a decrease in CIE y with increasing Al/O content (z). Broadening was computationally observed over a larger z range ($z = 0.125$ to $z = 0.167$) by Wang *et. al.*,[16] and the present work observes similar behavior for nominal Al/O amounts of $z = 0.050$ to $z = 0.125$. While an increase in the unit cell volume does not guarantee an increase in Eu-N/O bond distances, we observed an increase in the average bond length around the Eu site from our refinements of X-ray diffraction data. The Eu–N/O bond lengths of the activator site are observed to increase from 2.6710 Å in $z = 0.050$ to 2.6982 Å in $z = 0.125$ assuming an atomic position of $(0,0,\frac{1}{3})$, which lowers the crystal field splitting and results in the broadening of FWHM of the emission due to an increase in the splitting
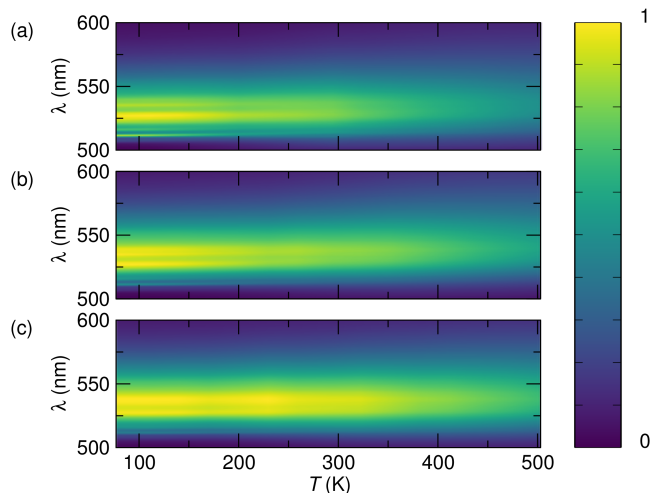
Fig. 7 Temperature dependent emission intensity is robust across the temperature range for $z = 0.050$ (a), $z = 0.075$ (b), and $z = 0.125$ (c) due to the rigid network of $(Si,Al)(O,N)_4$ tetrahedra and low Eu doping.

Fig. 8 Relative intensities of the temperature dependent emission demonstrate higher relative emission intensity at higher temperatures for $z = 0.075$ and $z = 0.125$. Relative emission intensity was computed by taking the integral of the emission profile at each temperature, and dividing by the maximum value for a given sample, which was different for each sample. Shared standard error (displayed next to legend) are ± 0.02.

between the topmost two $4f$ bands. Based on conventional models of phosphor crystal field splitting,[3,28] nitrides are generally more covalent than oxides and therefore should produce a larger centroid shift than oxides. A larger centroid shift leads to a closer proximity of the d and f levels, resulting in a lower energy difference between the $5d$ and $4f$ levels and longer wavelength emission. However, the expected trends based on covalency are not observed here and are likely instead dominated by polyhedral distortion, which is corroborated by recent work on this system.[16,23] Peak positions and FWHM values of Guassian fits of the emission data (Table 2) show a red shift an a slight broadening over the small z range investigated presently, corroborated by recent results on this system investigating photoluminescence behavior at low temperature and high pressure.[23]

For a given z value, more Eu substitution leads to concentration quenching, or a drop in the normalized emission intensity as a function of temperature.[29] Therefore, in the present work, β-$Si_{6-z}Al_zO_zN_{8-z}$:Eu^{2+} with a nominal composition of 0.9 mol% Eu is studied as the relatively low dopant concentration minimizes the effects of thermal quenching. Temperature-dependent photoluminescence measurements were employed to assess the thermal stability of the phosphors (Figure 7). All samples exhibit robust thermal stability due to the rigid network of $(Si,Al)(O,N)_4$ tetrahedra[6] and the large gap (>0.5 eV)[16] between the $5d$ levels and the host conduction band. Thermal quenching occurs when the $5d$ electron in the excited $4f^65d^1$ state is promoted to the conduction band of the host instead of relaxing to the $4f$ band.[30] The energy barrier for thermal ionization was calculated to increase with increasing z from 0.125 to 0.167 and then decrease with increasing z from 0.167 to 0.208.[16] The authors were unable to explain this discrepancy between calculation and experiment aside from noting that the barrier is high and the range they studied was more narrow than experimental investigations.[6,29] The present work experimentally observes the anomalous increase in thermal stability for increasing z over the range of 0.050 to 0.125, with $z = 0.125$ showing the most robust thermal stability up to
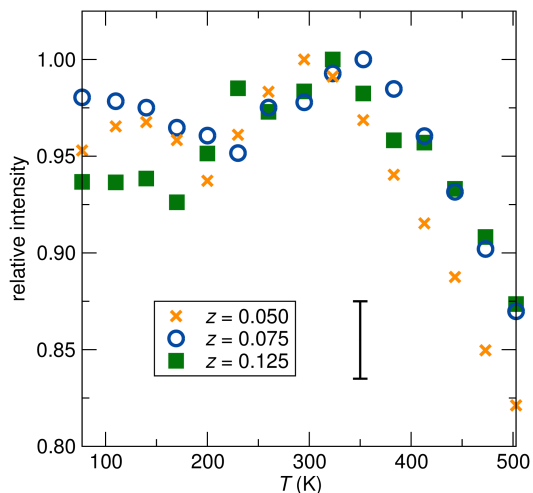
500 K. Comparing values for normalized intensity show that both $z = 0.075$ and $z = 0.125$ have higher relative emission intensity at higher temperatures than $z = 0.050$ (Figure 8). The low amount of Eu doping (0.09 mol-% nominally) also helps prevent thermal quenching by energy migration, which occurs in phosphors with higher doping[31] and likely does not occur in the present system as there exists no evidence for activator clustering with the low amounts of Eu dopants explored presently.[6] Fine structure features are observed and are more prominent for lower z at lower temperatures, which arise from the discrete ^7F_J states in Eu^{2+} assuming the Eu^{2+} is bonded ionically and the Eu^{2+} excited state is localized near the $4f$ orbital.[32]

Following the work of Dorenbos,[30] the activation energy for thermal quenching (ΔE) can be calculated using temperature-dependent emission intensity as a function of temperature by applying the following equation:

$$\ln\left[\frac{I(0)}{I(T)} - 1\right] = \frac{1}{k_B T}\Delta E + \ln\frac{\Gamma_0}{\Gamma_v}$$

where $\frac{I(0)}{I(T)}$ is the ratio of the highest intensity in the measured range $I(0)$ to the intensity at a particular temperature $I(T)$, k_B is the Boltzmann constant, T is temperature, Γ_v is the radiative decay rate of the $5d$ state of the activator, and Γ_0 is the attempt rate for thermal quenching. Linear fits of temperature-dependent intensity can then be used to calculate ΔE (Figure 9).

In the present work, linear fits of the data from 323 K to 503 K reveals that the calculated ΔE for $z=0.05$, $z=0.075$, and $z=0.125$ is 0.06 eV, 0.25 eV, and 0.20 eV, respectively. Compositions $z=0.075$ and $z=0.125$ match well with reported values (0.234 eV),[33] which support the observed high resistance to thermal quenching in this system. Data for the entire temperature range measured presently was not accurately captured with a
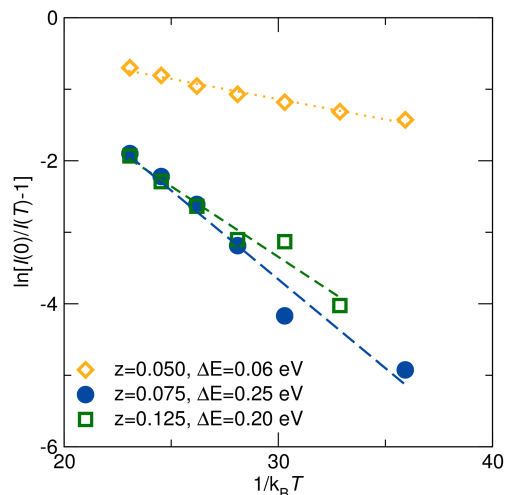
Fig. 9 Linear fits of $\ln[I(0)/I(T) - 1]$ vs. $\frac{1}{k_B T}$ from 323 K to 503 K were used to calculate activation energy of thermal quenching (ΔE) and show relatively high activation energies for $z=0.075$ and $z=0.125$.

Fig. 10 Room temperature PLQY collected with λ_{ex} = 405 nm and λ_{ex} = 450 nm for the β-$Si_{6-z}Al_zO_zN_{8-z}$:$Eu_{0.009}$ series. Highest efficiency is observed in the highest z sample at both excitation wavelengths. Error bars represent the standard deviation for measurements on three separate samples, and lines were added to guide the eye.

linear fit due to oscillations in the emission intensity as a function of temperature, which is corroborated by recent work on this system[23] and is one possible reason for the discrepancy in the $z=0.050$ sample. This intensity increase and decrease has also been observed in canonical Ce-doped YAG phosphors for both emission and lifetime, wherein radiative recombination dominates up to a certain temperature (around 523 K) before dropping off due to thermal quenching.[34,35] The current work observes the same behavior in the β-SiAlON system in addition to robust thermal quenching resistance.

PLQY was measured for both λ_{ex} = 405 nm and λ_{ex} = 450 nm (Figure 10). When comparing different compositions at room temperature, we see that PLQY increases with increasing z and that high PLQY values are achieved for both violet and blue excitation. The origins of this trend are likely linked to the calculated high barrier for thermal ionization (0.56-0.68 eV) that increases with increasing z from 0.125 to 0.167.[16] The increasing barrier calculated by Wang *et. al.* results in a high energy penalty for excited states to be promoted to the conduction band instead of relaxing to the 4f band to emit a photon. This limits nonradiative processes for increasing z across the small range studied, and offers a possible explanation for the origin of maximum PLQY (92%) observed for the $z = 0.125$ sample in our work. Additionally, the high ratio of Eu^{2+} to Eu^{3+} observed using XANES contributes to the high absolute PLQY values measured for β-$Si_{6-z}Al_zO_zN_{8-z}$:Eu^{2+} phosphors.

4 Conclusions

Specific emission properties can be targeted via compositional tuning, such as narrower emission β-SiAlON:Eu^{2+} (low z) for lower temperature operation, or maximum PLQY and improved thermal stability (higher z up to 0.125) for high flux and/or high temperature operation. We have provided experimental evidence on the role of increasing z at low concentrations in β-$Si_{6-z}Al_zO_zN_{8-z}$:Eu^{2+} in modifying the structure and the resulting optical properties. XANES was used to confirm that the ma-
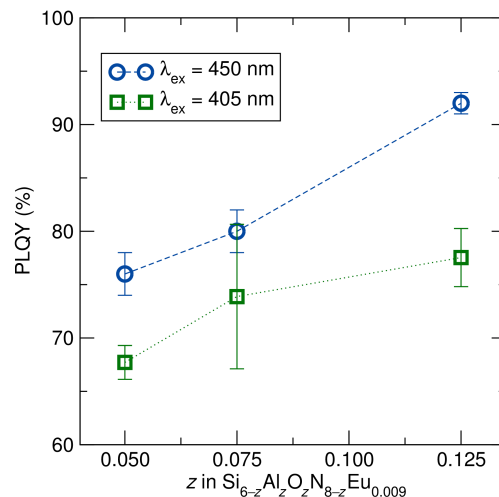
jority of Eu in the structure is in the active Eu^{2+} state, which allows for further investigation of the role of varying z as any observed changes in optical properties are not due to differences in Eu valence between samples. Increasing z distorts the Eu-N/O_9 environment, resulting in a red shift and broadening of emission. Temperature-dependent emission for these samples are robust with an increase in thermal stability with increasing z, due to the large gap between 5d levels and the conduction band of the host. Increased thermal quenching resistance is observed with increasing z over a small range, and likely gives rise to the increased quantum yield due to the predicted high barrier for thermal ionization that increases with increasing z. The present work provides experimental verification of optical properties resulting from an increase in the polyhedral distortion of the Eu^{2+} activator site with increasing Al/O content, as well as enhanced thermal stability due to a large thermal ionization barrier. Our work illustrates that structurally tuning the host lattice at low concentrations can be leveraged to optimize the optical and thermal performance of this important inorganic phosphor.

5 Acknowledgements

Research Facilities Network (www.mrfn.org).

References

1 S. Nakamura, T. Mukai and M. Senoh, *Appl. Phys. Lett.*, 1994, **64**, 1687–1689.

2 S. Pimputkar, J. S. Speck, S. P. DenBaars and S. Nakamura, *Nat. Photon.*, 2009, **3**, 180–182.

3 N. C. George, K. A. Denault and R. Seshadri, *Annu. Rev. Mater. Res.*, 2013, **43**, 481–501.

4 J. Sheu, S. Chang, C. Kuo, Y. Su, L. Wu, Y. Lin, W. Lai, J. Tsai, G. Chi and R. Wu, *IEEE Photon. Technol. Lett.*, 2003, **15**, 18–20.

5 N. Hirosaki, R.-J. Xie, K. Kimoto, T. Sekiguchi, Y. Yamamoto, T. Suehiro and M. Mitomo, *Appl. Phys. Lett.*, 2005, **86**, 211905.

6 J. Brgoch, M. W. Gaultois, M. Balasubramanian, K. Page, B.-C. Hong and R. Seshadri, *Appl. Phys. Lett.*, 2014, **105**, 181904.

7 W. B. Im, N. N. Fellows, S. P. DenBaars and R. Seshadri, *J. Mater. Chem.*, 2009, **19**, 1325–1330.

8 K. A. Denault, N. C. George, S. R. Paden, S. Brinkley, A. A. Mikhailovsky, J. Neuefeind, S. P. DenBaars and R. Seshadri, *J. Mater. Chem.*, 2012, **22**, 18204–18213.

9 A. P. Black, K. A. Denault, C. Frontera, R. Seshadri, A. R. Goñi and A. Fuertes, *J. Mater. Chem. C*, 2015, **3**, 11471–11477.

10 J. Brgoch, S. P. DenBaars and R. Seshadri, *J. Phys. Chem. C*, 2013, **117**, 17955–17959.

11 K. A. Denault, J. Brgoch, S. D. Kloß, M. W. Gaultois, J. Siewenie, K. Page and R. Seshadri, *ACS Appl. Mater. Interfaces*, 2015, 150327101213007.

12 K. A. Denault, M. Cantore, S. Nakamura, S. P. DenBaars and R. Seshadri, *AIP Adv.*, 2013, **3**, 072107.

13 Q.-Q. Zhu, X.-J. Wang, L. Wang, N. Hirosaki, T. Nishimura, Z.-F. Tian, Q. Li, Y.-Z. Xu, X. Xu and R.-J. Xie, *J. Mater. Chem. C*, 2015, **3**, 10761–10766.

14 K. Kimoto, R.-J. Xie, Y. Matsui, K. Ishizuka and N. Hirosaki, *Appl. Phys. Lett.*, 2009, **94**, 041908.

15 C. Cozzan, K. J. Griffith, G. Laurita, J. G. Hu, C. P. Grey and R. Seshadri, *Inorg. Chem.*, 2017, **56**, 2153–2158.

16 Z. Wang, W. Ye, I.-H. Chu and S. P. Ong, *Chem. Mater.*, 2016, **28**, 8622–8630.

17 T. Nakayasu and T. Yamada, *Acta Crystallogr., Sect. B: Struct. Sci.*, 1997, **80**, 1195–1215.

18 W. H. Baur, *Acta Cryst.*, 1974, **B30**, 1195–1215.

19 K. Momma and F. Izumi, *J. Appl. Crystallogr.*, 2008, **41**, 653–658.

20 B. Ravel and M. Newville, *J. Synchrotron Radiat.*, 2005, **12**, 537–541.

21 J. C. de Mello, H. F. Wittmann and R. H. Friend, *Adv. Mater.*, 1997, **9**, 230–232.

22 I. D. Brown, *Chem. Rev.*, 2009, **109**, 6858–6919.

23 X. Zhang, M.-H. Fang, Y.-T. Tsai, A. Lazarowska, S. Mahlik, T. Lesniewski, M. Grinberg, W. K. Pang, F. Pan, C. Liang, W. Zhou, J. Wang, J.-F. Lee, B.-M. Cheng, T.-L. Hung, Y.-Y. Chen and R.-S. Liu, *Chem. Mater.*, 2017.

24 H. Höppe, H. Lutz, P. Morys, W. Schnick and A. Seilmeier, *J. Phys. Chem. Solids*, 2000, **61**, 2001–2006.

25 J. Van Krevel, J. Van Rutten, H. Mandal, H. Hintzen and R. Metselaar, *J. Solid State Chem.*, 2002, **165**, 19–24.

26 R.-J. Xie, M. Mitomo, K. Uheda, F.-F. Xu and Y. Akimune, *J. Am. Ceram. Soc.*, 2002, **85**, 1229–1234.

27 J. L. Wu, G. Gundiah and A. Cheetham, *Chem. Phys. Lett.*, 2007, **441**, 250–254.

28 P. Dorenbos, *J. Alloys Compd.*, 2002, **341**, 156–159.

29 R.-J. Xie, N. Hirosaki, H.-L. Li, Y. Q. Li and M. Mitomo, *J. Electrochem. Soc.*, 2007, **154**, J314–J319.

30 P. Dorenbos, *J. Phys. Condens. Matter*, 2005, **17**, 8103.

31 V. Bachmann, C. Ronda and A. Meijerink, *Chem. Mater.*, 2009, **21**, 2077–2084.

32 K. Takahashi, K.-i. Yoshimura, M. Harada, Y. Tomomura, T. Takeda, R.-J. Xie and N. Hirosaki, *Sci. Tech. Adv. Mater.*, 2012, **13**, 015004.

33 J. H. Ryu, Y.-G. Park, H. S. Won, S. H. Kim, H. Suzuki, J. M. Lee, C. Yoon, M. Nazarov and B. Tsukerblat, *J. Electrochem. Soc.*, 2007, **155**, J99–J104.

34 J. Ueda, P. Dorenbos, A. J. Bos, A. Meijerink and S. Tanabe, *J. Phys. Chem. C.*, 2015, **119**, 25003–25008.

35 S. Arjoca, E. G. Víllora, D. Inomata, K. Aoki, Y. Sugahara and K. Shimamura, *Mater. Res. Express*, 2015, **2**, 055503.